

NUMERICAL SOLUTION OF THE BELTRAMI EQUATION VIA A PURELY LINEAR SYSTEM

R. Michael Porter¹

Department of Mathematics,
Centro de Investigación y de Estudios Avanzados del I.P.N.,
Apdo. Postal 1-798, Arteaga 5, 76000 Querétaro, Qro., Mexico
mike@math.cinvestav.edu.mx

Hirokazu Shimauchi²

Division of Mathematics,
Graduate School of Information Sciences, Tohoku University
6-3-09 Aramaki-Aza-Aoba, Aoba-ku, Sendai 980-8579, Japan
shimauchi@ims.is.tohoku.ac.jp, hirokazu.shimauchi@gmail.com

Keywords: numerical quasiconformal mapping, numerical conformal mapping,
Beltrami equation, quadratic differential, triangular mesh.

AMS subject classification: 30C62

Abstract

An effective algorithm is presented for solving the Beltrami equation $\partial f/\partial\bar{z} = \mu \partial f/\partial z$ in a planar disk. The disk is triangulated in a simple way and f is approximated by piecewise linear mappings; the images of the vertices of the triangles are defined by an overdetermined system of linear equations. (Certain apparently nonlinear conditions on the boundary are eliminated by means of a symmetry construction.) The linear system is sparse and its solution is obtained by standard least-squares, so the algorithm involves no evaluation of singular integrals nor any iterative procedure for obtaining a single approximation of f . Numerical examples are provided, including a deformation in a Teichmüller space of a Fuchsian group.

1 Introduction

The Beltrami equation

$$\frac{\partial f(z)/\partial\bar{z}}{\partial f(z)/\partial z} = \mu(z) \tag{1}$$

determines a unique normalized quasiconformal self-mapping f of the unit disk $\mathbb{D} = \{z: |z| < 1\}$ in the complex plane. Here μ is a given measurable function in

¹Research partially supported by CONACyT grant 166183

²Research supported by International Advanced Research and Education Organization in Tohoku University

\mathbb{D} with $\|\mu\|_\infty < 1$, and is called the Beltrami derivative (or complex dilatation) of f . One says that f is μ -conformal.

The Beltrami equation has been the object of deep investigation in large measure due to its importance in the theory of deformations of Kleinian groups and their applications to Teichmüller spaces [13, 17]. Other applications of the Beltrami equation as mentioned in the introduction to [7] are quite well known and we will not go into them here. Some more recent applications, such as mapping of the cerebral cortex, use the Beltrami equation in the spirit of its original application, dating back to Gauss, for finding a conformal mapping from a surface in 3-space onto a planar region; this is done effectively in [2] although without explicit use of the Beltrami derivative μ . The Beltrami derivative has also been proposed as a way of compressing data for surface maps [20].

With this increasing use of computer applications it has become of great interest to know how solve the Beltrami equation numerically. One method for doing this is suggested naturally by the classical existence proof given by Moriyoyarskii-Ahlfors-Bers [13, 17]. For this method one must evaluate singular integrals of the form

$$T_m g(z) = -\frac{1}{\pi} \iint_{\mathbb{D}} \frac{g(\zeta)}{(\zeta - z)^m} d\xi d\eta, \quad m = 1, 2$$

(defined as Cauchy principal values when $m = 2$), and then calculate sums of Neumann series of the form $\sum T_2(\mu T_2(\cdots(\mu T_2(\mu)\cdots)))$. A related approach involving the singular integrals was developed by P. Daripa and D. Mashat [6, 7], and refined by D. Gaidashev and D. Khmelev [11]. Instead of summing the Neumann series, their method involves iteration towards a solution of a related Dirichlet problem. Their work includes refinement of the technique of evaluation of the singular integrals via FFT, which is of interest in itself.

Zh.-X. He [14] proposed an alternative method of solving the Beltrami equation, based on circle packings. G. B. Williams [28] presented another circle-packing method, based on the idea of conformal welding. Little information is available on the numerical performance of these methods. Lui et. al [21] describe yet another method, which reduces the question of solving the Beltrami equation to that of a linear system on the underlying mesh. Their method, focused on obtaining Teichmüller mappings of prescribed domains (rather than self-mappings of a disk as we consider here), is applied to problems of face recognition and brain mapping. Many other approaches have been given to solve for quasiconformal mappings, often from surfaces in \mathbb{R}^3 to the plane. Descriptions and further references may be found in [12, 19]. An attempt to solve the numerical solution of the Beltrami equation by applying conformal mappings as an intermediate step, was made in [23]. However, this method was later found not to converge to the proper solution and appears not to be salvageable.

In this paper we give a much simpler algorithm with full proof of convergence in the case of a smooth Beltrami derivative. (We believe that this smoothness condition is overly restrictive, as numerical experiments suggest.) In Section

2 we gather the basic facts we will need about quasiconformal mappings. In Sections 3 and 4 we explain how to set up the linear system describing the Beltrami equation. In Section 5 the algorithm is specified and the main theorem on the convergence of the algorithm is stated and proved. Several numerical examples are provided in Section 6, including a deformation of a Fuchsian group. In the closing comments we discuss the corresponding computational cost.

2 Preliminaries

2.1 Affine linear quasiconformal mappings

In this section μ, a, b are complex constants subject to $a \neq 0, |\mu| < 1$, and we consider the mappings

$$L_\mu(z) = \frac{z + \mu\bar{z}}{1 + \mu}, \quad (2)$$

$$H_{a,b}(z) = az + b, \quad (3)$$

for $z \in \mathbb{C}$. Thus L_μ is μ -conformal and real-linear, while $H_{a,b}$ is conformal and affine complex-linear. Note that L_μ is determined by its value at any single point other than its fixed points $z = 0$ and $z = 1$, while $H_{a,b}$ is determined by the images of any two points. All μ -conformal affine linear mappings are of the form $H_{a,b} \circ L_\mu$, and this decomposition is unique. We will use the following form of expressing affine linear mappings.

Proposition 2.1 *Given z_1, z_2 distinct and w_1, w_2 distinct, together with $|\mu| < 1$, there is a unique μ -conformal affine linear mapping $B = B_{\mu; z_1, z_2; w_1, w_2}$ which sends z_1 to w_1 and z_2 to w_2 . This mapping is given explicitly by*

$$\begin{aligned} B(z) &= w_1 + \frac{w_2 - w_1}{L_\mu(z_2 - z_1)} L_\mu(z - z_1) \\ &= \frac{L_\mu(z_2 - z)}{L_\mu(z_2 - z_1)} w_1 + \frac{L_\mu(z_1 - z)}{L_\mu(z_1 - z_2)} w_2. \end{aligned}$$

The coefficients of w_1, w_2 in this last expression are never 0, 1, or ∞ when z_1, z_2, z_3 are distinct. As we will be interested in mappings of triangles, the following facts will be useful.

Corollary 2.2 *If a μ -conformal affine linear map takes z_1, z_2, z_3 to w_1, w_2, w_3 respectively, then*

$$L_\mu(z_2 - z_3) w_1 + L_\mu(z_3 - z_1) w_2 + L_\mu(z_1 - z_2) w_3 = 0.$$

Corollary 2.3 *Given z_1, z_2, z_3 noncollinear and w_1, w_2, w_3 noncollinear, there is a unique affine linear mapping which sends z_i to w_i ($i = 1, 2, 3$). Its Beltrami derivative is equal to*

$$\mu = -\frac{(z_2 - z_1)(w_3 - w_1) - (z_3 - z_1)(w_2 - w_1)}{(\overline{z_2 - z_1})(w_3 - w_1) - (\overline{z_3 - z_1})(w_2 - w_1)}. \quad (4)$$

Proof. The affine linear mapping is well-defined because each of the pairs $(z_2 - z_1, z_3 - z_1), (w_2 - w_1, w_3 - w_1)$ is linearly independent over the real numbers. To calculate the Beltrami derivative, substitute (2) into the formula of Corollary 2.2 and solve for μ . \square

In applying Corollary 2.3, one normally would also require the z - and w -triangles to be like-oriented, to ensure that $|\mu| < 1$.

2.2 Closeness to similarity

The affine-conformal mapping (3) sends triangles to similar triangles. A Beltrami derivative (4) can be regarded as a measure of how much the (positively oriented) triangles with vertices z_1, z_2, z_3 and w_1, w_2, w_3 fail to be similar. Indeed, these triangles may be carried by conformal mappings of the form $H_{a,b}$ to normalized triangles $(0, 1, c_0), (0, 1, c)$ respectively, which in turn correspond under the mapping L_μ where

$$\mu = -\frac{c - c_0}{c - \overline{c_0}}. \quad (5)$$

With c_0 fixed, the relation $c \leftrightarrow \mu$ from $\text{Im } c > 0$ to $|\mu| < 1$ thus associates an element of the unit disk to each similarity class of oriented triangles, and we can use $|\mu|$ as a measure of the discrepancy from being similar to the original triangle. In this regard we must note that the Beltrami derivative of the affine mapping from (z_1, z_2, z_3) to (w_1, w_2, w_3) is $e^{2i \arg(z_2 - z_1)} \mu$ (Proposition 2.6 below), so the absolute value is not altered by the normalization to the triangle $(0, 1, c_0)$ with horizontal base.

2.3 Quasiconformal mappings

The following well known general properties of quasiconformal mappings [1, 17, 18] are fundamental to this work.

Proposition 2.4 *If μ is measurable in $\mathbb{D} = \{z \in \mathbb{C} : |z| < 1\}$ and satisfies $\|\mu\|_\infty < 1$, then there is a unique μ -conformal mapping $f: \mathbb{D} \rightarrow \mathbb{D}$ satisfying the normalization*

$$f(0) = 0, \quad f(1) = 1.$$

Proposition 2.5 *Let μ, μ_n be measurable functions in \mathbb{D} with $\|\mu_n\|_\infty \leq c < 1$ and suppose that $\mu_n \rightarrow \mu$ pointwise as $n \rightarrow \infty$. Let f, f_n be the normalized solutions of the corresponding Beltrami equations given by Proposition 2.4. Then f_n converge to f uniformly on compact subsets of \mathbb{D} .*

Proposition 2.6 *Let f_1, f_2 be μ_1, μ_2 -conformal mappings respectively.*
(i) Suppose that f_1, f_2 are defined in the same planar domain and

$$f_2 = h \circ f_1.$$

Then $\mu_1 = \mu_2$ a.e. if and only if h is a conformal mapping from the image of f_1 to the image of f_2 .

(ii) Suppose that h is defined in the domain of f_2 and

$$f_2 = f_1 \circ h.$$

If h is conformal, then $\mu_2 = (\mu_1 \circ h)(\overline{h'}/h')$.

(iii) If

$$f_2(z) = \overline{f_1(\overline{z})},$$

then $\mu_2(z) = \overline{\mu_1(\overline{z})}$.

3 Context for discrete Beltrami equation

In this section we describe the geometric and algebraic elements necessary for our discrete version of the Beltrami equation.

To discretize the problem, we will consider finite triangulations \mathcal{T}_z of the closed unit disk $\overline{\mathbb{D}}$ in the z -plane. We always assume that the union $|\mathcal{T}_z|$ of the (closed) triangles of \mathcal{T}_z is bounded by a Jordan polygon inscribed in $\overline{\mathbb{D}}$. We are given a proposed Beltrami derivative μ in \mathbb{D} , i.e., a measurable function such that $\|\mu\|_\infty = \text{ess sup}_{z \in \mathbb{D}} |\mu(z)| < 1$, and we want to construct an isomorphic (simplicially equivalent) triangulation \mathcal{T}_w of the unit disk in the w -plane such that the induced piecewise linear mapping (PL-mapping) is approximately μ -conformal on each triangle $\tau \in \mathcal{T}_z$.

3.1 Logarithmic coordinates

Given μ , in many cases it is not difficult to find a discrete μ -conformal mapping to some triangulation \mathcal{T}_w of a domain whose shape is not predetermined, but the challenge is to make the outer polygon bounding \mathcal{T}_w precisely a circle. This question can be approached many ways, and in general the condition that “the points of the outer polygon of \mathcal{T}_z must be mapped to a circle centered at the origin” translates into some nonlinear conditions. In order to evade this “outer boundary condition” we can extend $\mu(z)$ by reflection to the exterior of \mathbb{D} (using the Chain Rule for Beltrami derivatives), likewise extending \mathcal{T}_z by including the

vertices $1/\overline{z_{jk}}$, and then solve the extended problem on the Riemann sphere. However, the nonlinearity of the inversion $1/\overline{z}$ leads to inaccuracies since it does not respect affine mappings between triangles. In other words, the inversion in $\{|z| = 1\}$ does not produce a truly symmetric discrete problem. We prefer to avoid this difficulty as follows, by introducing logarithmic coordinates in the form of the variables $Z = \log z$, $W = \log w$ in the left half-plane (cf. [18, section 6.4]). In other words, in order to solve for the discrete function $w = f(z)$ from \mathbb{D} to \mathbb{D} we will solve first for the correspondence

$$W = F(Z) \tag{6}$$

where $\exp F(Z) = f(\exp z)$, and then simply apply the operation

$$z = \exp(Z), \quad w = \exp(W) \tag{7}$$

to obtain the desired mapping $z \mapsto w$. Of course, we will need to justify that the distortion of triangles produced by the exponential mapping does not affect the accuracy significantly.

3.2 Triangulation

It is convenient to use negative indices for points of the basic domain. We fix the mesh order, that is, a pair of positive integers M, N (presumably large). Let

$$R_{-M} < R_{-M+1} < \dots < R_{-1} < R_0 = 0$$

and define the $(M + 1)N$ vertices

$$Z_{jk} = R_j + \frac{2\pi(k + j_2/2)}{N}i \tag{8}$$

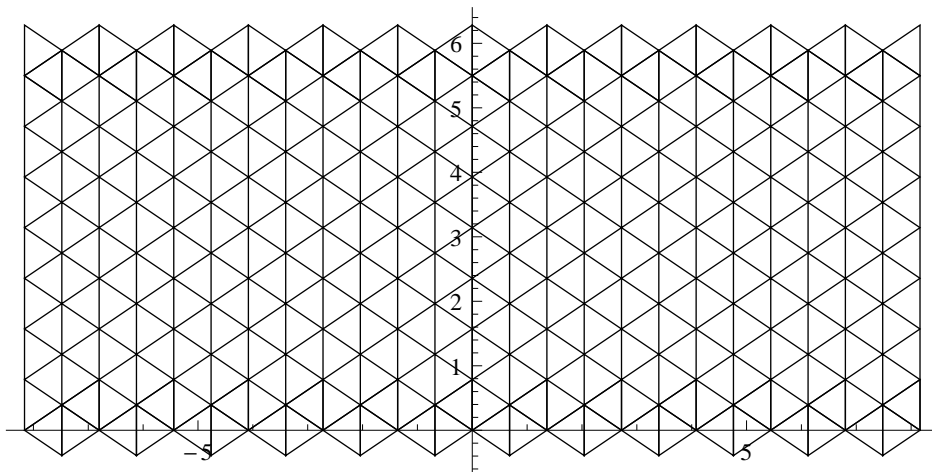


Figure 1: Basic mesh in W -plane, with its reflection in the imaginary axis.

for $-M \leq j \leq 0$ and $0 \leq k \leq N-1$. Here $j_2 = j \bmod 2$ is 0 when j is even and 1 when j is odd.

If we extend the formula for arbitrary values of k , we obtain a periodic mesh with $Z_{j,k+N} = Z_{jk} + 2\pi i$. The basic mesh contains MN *rightward pointing triangles* defined as follows,

$$\tau_{jk}^+ = \begin{cases} (Z_{j-1,k-1}, Z_{j-1,k}, Z_{j,k}), & j \text{ even,} \\ (Z_{j-1,k}, Z_{j-1,k+1}, Z_{j,k}), & j \text{ odd,} \end{cases} \quad (9)$$

for $-M+1 \leq j \leq 0$. There are also MN *leftward pointing triangles*

$$\tau_{jk}^- = \begin{cases} (Z_{j+1,k-1}, Z_{j+1,k}, Z_{j,k}), & j \text{ even,} \\ (Z_{j+1,k}, Z_{j+1,k+1}, Z_{j,k}), & j \text{ odd,} \end{cases} \quad (10)$$

for $-M \leq j \leq -1$. Note however, that for even values of j the triangle τ_{j0}^+ contains $Z_{j-1,-1}$ and the triangle τ_{j0}^- contains $Z_{j+1,-1}$; while for odd j the triangle $\tau_{j,N-1}^+$ contains $Z_{j-1,N}$ and the triangle $\tau_{j,N-1}^-$ contains $Z_{j+1,N}$. The second index k of each of these points lie outside of the basic range $0 \leq k \leq N-1$ which most interests us.

We will assume for the rest of this paper that

$$R_j = (\sqrt{3}\pi/N)j, \quad (11)$$

so the triangles τ_{jk}^\pm will be equilateral. We extend the structure to the right half-plane using the reflection in the imaginary axis

$$\varrho(Z) = -\overline{Z}, \quad (12)$$

and setting

$$Z_{jk} = \varrho(Z_{-j,k})$$

for indices $j > 0$. Thus in the extended domain we have $-M \leq j \leq M$, with symmetry around the index $j = 0$. The extended triangulation contains $(2M+1)N$ vertices.

Since we are originally given μ in \mathbb{D} , we will need the pullback of μ as a differential of type $(-1, 1)$ to the left half-plane (Proposition 2.6), that is,

$$\nu(Z) = \mu(e^Z) \frac{e^{\overline{Z}}}{e^Z} = \mu(e^Z) e^{-2i \operatorname{Im} Z}, \quad \operatorname{Re} Z < 0. \quad (13)$$

For $\operatorname{Re} Z > 0$ we want $F(Z) = \rho(F(\rho(Z)))$ according to (6). By Proposition 2.6 the Beltrami derivative of F is $\nu(Z) = \nu(\varrho(Z))$. We will write ν_{jk}^\pm for the average value of $\nu(Z)$ on the triangle τ_{jk}^\pm . While technically this means the integral of ν divided by the area of the triangle, for numerical work it is convenient to take the average of $\nu(Z)$ over the three vertices as an approximation to this integral, at least when ν is continuous. Let us note that

$$\nu_{jk} = \overline{\nu_{-j,k}}, \quad j > 0. \quad (14)$$

3.3 Boundary conditions

We will need to describe the behavior of the discrete μ -conformal mapping at the points corresponding to $j = \pm M$. The vertical line $\{Z: \operatorname{Re} Z = R_{-M}\}$ corresponds to the circle $|z| = r_{-M}$ in the z -plane, where we write $r_j = \exp R_j$. Let $f: \mathbb{D} \rightarrow \mathbb{D}$ denote the exact (smooth) solution of (1), normalized by $f(0) = 0$, $f(1) = 1$. Then near $z = 0$, we know (recall (2), (3)) that f is approximately equal to an affine map $H_{a,0} \circ L_{\mu(0)}$ for some $a \in \mathbb{C} \setminus \{0\}$, and the image of the small circle is an ellipse in the w -plane whose eccentricity is determined by $\mu(0)$ and whose size is determined by a . Similarly, the right boundary $\{\operatorname{Re} Z = R_M\}$ corresponds to the inversion of this small ellipse in the circumference $\partial\mathbb{D}$ of \mathbb{D} . Thus we are considering the problem as defined in the annulus $1/r_M \leq |z| \leq r_M$, and the value $|a|$ is related to the conformal module [18] of the image of this annulus under f . We will sidestep the question of explicitly considering a in 4.2 below.

4 Discrete Beltrami equation

Here we define the system of linear equations representing the solution of the Beltrami equation. First we consider the unknowns

$$\{W_{jk}: -M \leq j \leq 0, 0 \leq k \leq N-1\}$$

in the left half-plane.

4.1 Triangle equations

Following Corollary 2.2, to each rightward pointing triangle τ_{jk}^+ of (9) we associate one linear equation

$$a_{jk}^+ W_{jk} + b_{jk}^+ W_{j-1,k} + c_{jk}^+ W_{j-1,k+1} = 0 \quad (15)$$

where

$$\begin{aligned} a_{jk}^+ &= \begin{cases} L_{\nu_{jk}}(Z_{j-1,k-1} - Z_{j-1,k}), & j \text{ even,} \\ L_{\nu_{jk}}(Z_{j-1,k} - Z_{j-1,k+1}), & j \text{ odd,} \end{cases} \\ b_{jk}^+ &= \begin{cases} L_{\nu_{jk}}(Z_{j-1,k} - Z_{j,k}), & j \text{ even,} \\ L_{\nu_{jk}}(Z_{j-1,k+1} - Z_{j,k}), & j \text{ odd,} \end{cases} \\ c_{jk}^+ &= \begin{cases} L_{\nu_{jk}}(Z_{j,k} - Z_{j-1,k-1}), & j \text{ even,} \\ L_{\nu_{jk}}(Z_{j,k} - Z_{j-1,k}), & j \text{ odd,} \end{cases} \end{aligned} \quad (16)$$

and similarly an equation for each leftward pointing triangle τ_{jk}^- ,

$$a_{jk}^- W_{jk} + b_{jk}^- W_{j+1,k-1} + c_{jk}^- W_{j+1,k} = 0 \quad (17)$$

where

$$\begin{aligned}
a_{jk}^- &= \begin{cases} L_{\nu_{jk}}(Z_{j+1,k-1} - Z_{j+1,k}), & j \text{ even,} \\ L_{\nu_{jk}}(Z_{j+1,k} - Z_{j+1,k+1}), & j \text{ odd,} \end{cases} \\
b_{jk}^- &= \begin{cases} L_{\nu_{jk}}(Z_{j+1,k} - Z_{j,k}), & j \text{ even,} \\ L_{\nu_{jk}}(Z_{j+1,k+1} - Z_{j,k}), & j \text{ odd,} \end{cases} \\
c_{jk}^- &= \begin{cases} L_{\nu_{jk}}(Z_{j,k} - Z_{j+1,k-1}), & j \text{ even,} \\ L_{\nu_{jk}}(Z_{j,k} - Z_{j+1,k}), & j \text{ odd.} \end{cases}
\end{aligned} \tag{18}$$

However, while these equations stand as written for values of k giving triangles in the ‘‘interior’’ of our mesh, at the upper and lower parts of the mesh we must take the $2\pi i$ -periodicity into account in order to conserve our requirement that $0 \leq l \leq N-1$ in every appearance of W_{jl} . The exceptions to these equations occur when $k+1 = N+1$ in (15) and when $k-1 = -1$ in (17). When $k=0$ and j is even we should use $W_{j\pm 1, N-1} - 2\pi i$ in place of $W_{j\pm 1, -1}$, while when $k=N-1$ and j is odd we should write $W_{j\pm 1, 0} + 2\pi i$ instead of $W_{j\pm 1, N}$. Referring to (9) and (10) one sees that the exceptional equations are defined by

$$\begin{aligned}
a_{j0}^\pm W_{j0} + b_{j0}^\pm W_{j-1,0} + c_{j0}^\pm W_{j-1,1} &= -2\pi i c_{j0}^\pm, \quad j \text{ even,} \\
a_{j0}^\pm W_{j0} + b_{j0}^\pm W_{j-1,0} + c_{j0}^\pm W_{j-1,1} &= 2\pi i b_{j0}^\pm, \quad j \text{ odd.}
\end{aligned} \tag{19}$$

The next step is to ‘‘reflect’’ these equations to the right half-plane via (12). We want F to be symmetric in the imaginary axis, $F = \varrho F \varrho$. Since the Beltrami derivative of this composition is $\nu = \overline{\nu} \circ \varrho$, the prescription (14) indeed reflects ν appropriately to the right half-plane as a discrete Beltrami differential. In other words, consider a triangle $\tau_{jk}^\pm = \varrho(\tau_{-j,k}^\pm)$ in the right half Z -plane ($j \geq 0$). The image $F(\tau_{jk}^\pm)$ in the W -plane, defined by W_{jk} and two adjacent vertices, must be the same as $\varrho(F(\tau_{-j,k}^\pm))$. It is easily seen that the correspondence $\varrho(\tau_{jk}^\pm) \rightarrow \varrho(F(\tau_{jk}^\pm))$ translates into equations of the same form as (15), (17) with $j \geq 0$ and with the coefficients

$$a_{jk}^\pm = \overline{a_{-j,k}^\pm}, \quad b_{jk}^\pm = \overline{b_{-j,k}^\pm}, \quad c_{jk}^\pm = \overline{c_{-j,k}^\pm}. \tag{20}$$

So far we have described how the triangles of the extended Z -triangulation provide $4MN$ linear equations: $2MN$ from the left half-plane and another $2MN$ via (20).

4.2 Boundary equations

Next we look at the right and left boundary conditions. We return for a moment to the z -disk. The smallest polygon of the mesh is formed of points on the circle of radius $r_{-M} = \exp(R_{-M})$. Following the discussion in 3.3, let e_k be the images of these points under the real-linear mapping L_{μ_0} ,

$$e_k = L_{\mu_0}(r_{-M} e^{2\pi i k/N}) = r_{-M} L_{\mu_0}(e^{2\pi i k/N}), \quad 0 \leq k \leq N-1,$$

where μ_0 denotes the average value of $\mu(z)$ inside this circle. Thus the e_k lie on a small ellipse. Define

$$E_k = \log e_k \quad (21)$$

with $0 \leq \arg E_k < 2\pi$. It might seem natural to use the values E_k , $\varrho(E_k)$ as “boundary values” simply by adding equations $W_{-M,k} = E_k$, $W_{M,k} = -\overline{E_k}$. However, this will create the difficulty which was mentioned earlier related to the unknown conformal module of the region between the small ellipse and its inversion, because the value of $\log r_{-M}$ in our construction, which is the real part R_{-M} of E_k , is arbitrary as far as μ is concerned. Instead of that we want a condition which says that the image of the circle of radius r_{-M} is an unknown (complex nonzero) multiple of the ellipse $\{e_k\}$. In logarithmic coordinates, the condition is that the image of the curve $\{Z_{-M,k}\}_k$ is a translate of the curve $\{E_k\}_k$ by a complex constant. Similar considerations apply to the reflected curve $\{\varrho(E_k)\}_k$. The boundary equations which achieve this are the $2(N-1)$ equations

$$\begin{aligned} W_{-M,k} - W_{-M,k-1} &= D_k, \\ W_{M,k} - W_{M,k-1} &= \overline{D_k}, \end{aligned} \quad (22)$$

where $D_k = E_k - E_{k-1}$ and $1 \leq k \leq N-1$. Note that the magnitude of r_{-M} does not influence the value of D_k .

Finally, for normalization of the solution we add one more equation,

$$W_{0,0} = 0, \quad (23)$$

which is self-symmetric. This says that $F(0) = 0$, or equivalently, $f(1) = 1$.

5 Statement and proof of main theorem

The linear system outlined in section 4 has more equations than variables: there are $n_v = (2M+1)N$ unknowns W_{jk} , $-M \leq j \leq M$, $0 \leq k \leq N-1$, and $n_e = 4MN + 2(N-1) + 1$ equations. Therefore we will use the standard Least-Squares approximation [4] method to find a solution. To describe the system it is convenient to rename the variables in a single vector V with

$$V_p = W_{jk} \quad (24)$$

where $p = p(j, k)$ is given by an arbitrary but fixed bijective correspondence from the set of index pairs $\{(j, k)\}$ to the range $1 \leq p \leq n_v$. We will write $V = \underline{W}$ or $W = \underline{V}$ to indicate this renaming of the indices. The linear system now takes the form $A\underline{W} = B$ or

$$AV = B \quad (25)$$

where $A = (A_{np})$ is a complex $n_e \times n_v$ matrix and $B = (B_n)$ is a complex vector of length n_e . When considering the mesh $\{Z_{jk}\}$ as fixed, we will say that (A, B) is the *associated linear system* to the collection of ν -values $\{\nu_{jk}\}$ (recall that the coefficients depend both on ν_{jk} and Z_{jk}).

5.1 Statement of theorem

Our algorithm may be summarized briefly as follows:

1. Given a proposed Beltrami derivative μ in \mathbb{D} , choose the dimensions M, N for a triangular mesh $\{Z_{jk}\}$ in the Z -plane and calculate the averages ν_{jk} of the pullback of $\mu(z)$ to the Z -plane via (13).
2. Calculate the coefficients of the linear system (A, B) associated to $\{\nu_{jk}\}$ as prescribed by equations (15), (17), (19), (22), and (23).
3. Apply the method of Least Squares to calculate the approximation V of the solution of the system $AV = B$, and arrange the entries of V to form the mesh $\{W_{jk}\} = \underline{V}$.
4. Calculate $w_{jk} = \exp W_{jk}$ for $-M \leq j \leq 0$ and $0 \leq k \leq N - 1$. The desired mapping is the piecewise linear simplicial mapping such that $z_{jk} \mapsto w_{jk}$ where $z_{jk} = \exp Z_{jk}$.

As an illustration we show in Figure 2 the w -triangulation for the Beltrami derivative defined by $\mu(z) = 0.5$ when $\text{Im } z > 0$, and $\mu(z) = 0$ when $\text{Im } z \leq 0$. This was calculated with $(M, N) = (32, 32)$. Therefore there are many very small triangles which cannot be seen in the picture, in particular those adjacent

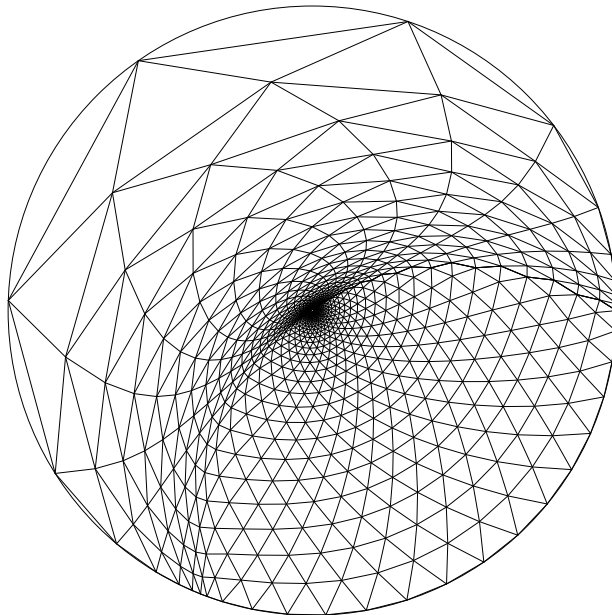


Figure 2: Different constants in upper and lower w -half-planes. Note the normalizations $f(0) = 0, f(1) = 1$.

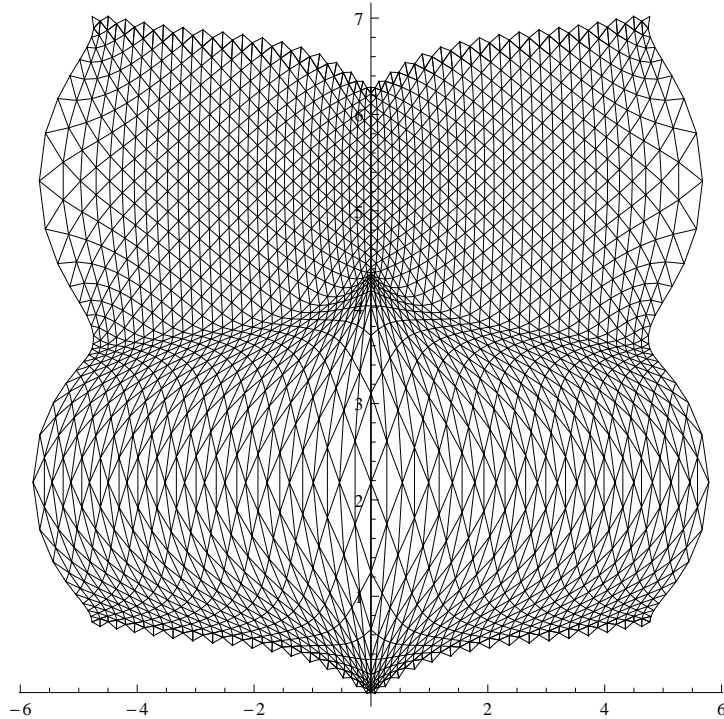


Figure 3: Different constants in upper and lower W -half-planes. Note the lifted ellipses at left and right extremes of the boundary.

to the small bounding ellipse. Note how the image triangles from the lower half-plane appear to be equilateral, and there is a clear dividing line between them and the stretched triangles from the upper half-plane. The stretched triangles are not mutually similar, even though μ is constant, since the similarity class of an image triangle depends upon both the value of μ and the slope of the base of the domain triangle. In Figure 3 we show the logarithmic W -domain. In this picture the equilateral triangles are in the upper part, with imaginary parts approximately from π to 2π (near the imaginary axis, they occupy a smaller range).

Our main result is formulated as follows. Recall that the real parts R_j of the vertices of the logarithmic meshes are given by (11).

Theorem 5.1 *Let μ be a C^1 function in \mathbb{D} with $\|\mu\|_\infty < 1$. Let $M_s, N_s \rightarrow \infty$ as $s \rightarrow \infty$, where these sequences satisfy*

$$c_1 N_s \log N_s \leq M_s \leq c_2 N_s \log N_s \quad (26)$$

for constants c_1, c_2 where $c_1 > 1/(\pi\sqrt{3})$. Then

- i. For large s , the points $\{z_{jk}^{(s)}\}$ and the points $\{w_{jk}^{(s)}\}$ produced by the algorithm form the vertex sets of isomorphic triangulations $\mathcal{T}_z^{(s)}$ and $\mathcal{T}_w^{(s)}$ of

the unit disk \mathbb{D} . Further, any fixed compact set $K \subset \text{int } \mathbb{D}$ is contained in the supports of $\mathcal{T}_z^{(s)}$ and of $\mathcal{T}_w^{(s)}$ for large s .

- ii. Let $f^{(s)}$ denote the piecewise-linear mapping of $\mathcal{T}_z^{(s)}$ to $\mathcal{T}_w^{(s)}$ which sends $z_{jk}^{(s)}$ to $w_{jk}^{(s)}$ as given by Corollary 2.3. Then the mappings $f^{(s)}$ converge to the solution f of the Beltrami equation (1), normalized by $f(0) = 0$, $f(1) = 1$, as $s \rightarrow \infty$, uniformly on compact subsets of \mathbb{D} .

5.2 Lemmas

In the Lemmas 5.2 to 5.4, (A, B) is the associated linear system for some fixed collection $\{\nu_{jk}\}$ satisfying $|\nu_{jk}| < 1$, with mesh dimensions M and N .

Since there are many more equations than variables involved, it is not surprising that the system is overdetermined:

Lemma 5.2 *If $X \in \mathbb{C}^{n_v}$ and $AX = 0$, then $X = 0$.*

Proof. We examine the role of different rows of A in $AX = 0$. Recall that we write \underline{X}_{jk} for $X_{p(j,k)}$. First note that there appear equations (22) for the ‘‘lifted ellipse,’’ with zero on the right-hand side in place of D_k and \overline{D}_k . These equations say that $\underline{X}_{-M,k+1} - \underline{X}_{-M,k} = 0$; i.e., all of the $\underline{X}_{-M,k}$ are now of the same value, say c . The equations (15), (19) for the rightward-pointing triangles with $j = -M + 1$ give us

$$a_{-M+1,k}^+ \underline{X}_{-M+1,k} + b_{-M+1,k}^+ \underline{X}_{-M,k} + c_{-M+1,k}^+ \underline{X}_{-M,k'} = 0$$

for suitable k' , and using what we have just proved for $j = -M$ and the facts that $a_{-M+1,k}^+ \neq 0$ (recalling the remark after Proposition 2.1) and $a_{-M+1,k}^+ + b_{-M+1,k}^+ + c_{-M+1,k}^+ = 0$ we deduce that $\underline{X}_{-M+1,k} = c$ for all k . Continuing this way we have $\underline{X}_{-j,k} = c$ for all k and $-M \leq j \leq 0$. The normalization equation $\underline{X}_{0,0} = 0$ says that $c = 0$ and then the symmetry gives $\underline{X}_{jk} = 0$ for all j, k . Thus $X = 0$. \square

Lemma 5.3 *Let $\{X^{(n)}\}$ be such that $AX^{(n)} \rightarrow 0$. Then $X^{(n)} \rightarrow 0$.*

Proof. Consider a subsequence of $\{X^{(n)}\}$ which converges to a limit X . By continuity $AX = 0$. By Lemma 5.2, $X = 0$. Thus we see that every convergent subsequence of $\{X^{(n)}\}$ converges to 0. If $\{X^{(n)}\}$ is bounded, then it indeed has a convergent subsequence, so it follows that $X^{(n)} \rightarrow 0$ as desired.

Suppose then that $\{X^{(n)}\}$ is not bounded. The maximum absolute value $|X_p^{(n)}|$ of an entry of $X^{(n)}$ occurs infinitely often for some fixed index p_0 . On the corresponding subsequence we have $|X_{p_0}^{(n)}| \rightarrow \infty$. Let

$$Y^{(n)} = \frac{1}{X_{p_0}^{(n)}} X^{(n)},$$

so $|Y^{(n)}| = 1$. Also

$$AY^{(n)} = \frac{1}{X_{p_0}^{(n)}} AX^{(n)} \rightarrow 0$$

on the subsequence, where $|X_{p_0}^{(n)}| > 1$ large n . Since $\{Y^{(n)}\}$ is bounded, by the previous paragraph $Y^{(n)} \rightarrow 0$, which contradicts $|Y^{(n)}| = 1$. Therefore this case does not occur. \square

Lemma 5.4 *For any $W = \{W_{jk}\}$ ($-M \leq j \leq M$, $0 \leq k \leq N - 1$), the symmetry relation*

$$A\overleftarrow{W} = A\underline{\varrho}(W)$$

holds, where $\overleftarrow{W}_{jk} = W_{-j,k}$, $\underline{\varrho}(W) = \{\varrho(W_{jk})\}$ and ϱ is defined by (12). Let V be the solution of the linear system (25) produced by the method of Least Squares. Then the entries of $W = \underline{V}$ satisfy the symmetry $W_{-j,k} = \varrho(W_{jk})$. In particular, the central values W_{0k} are purely imaginary.

Proof. The relation $A\overleftarrow{W} = A\underline{\varrho}(W)$ follows immediately from the previous symmetry relations such as (20). The method of Least Squares produces V which minimizes the L_2 -norm of the residual $\|AV - B\|_2$. By Lemma 5.2, A has full column rank, so this optimal V is unique [4]. Therefore $\overleftarrow{W} = \underline{\varrho}(W)$. \square

In the following, recall the distance between similarity classes of triangles discussed in 2.2.

Lemma 5.5 *Let $f: \overline{\mathbb{D}} \rightarrow \overline{\mathbb{D}}$ be a C^1 -diffeomorphism of the closed disk (i.e., the restriction of a diffeomorphism of larger domains). Let $0 < c < 1$. Then every sufficiently fine triangulation \mathcal{T}_z of \mathbb{D} , formed of triangles which are within c of being equilateral, has the property that the images under f of its vertices form the vertices of an isomorphic triangulation \mathcal{T}_w .*

Proof. We may suppose without loss of generality that f preserves orientation. It is sufficient to show that all triangles of \mathcal{T}_z are sent to triangles of the same orientation. Indeed, this implies that the induced PL-mapping f preserves the triangle structure locally, and hence is a local homeomorphism. Further, it is easily seen that $\hat{f}: |\mathcal{T}_z| \rightarrow |\mathcal{T}_w|$ satisfies the path-lifting property, and thus is a covering map of simply connected regions and hence a homeomorphism, so the triangulations are isomorphic.

If the affirmation were false, there would be a sequence $\{\mathcal{T}^{(n)}\}$ of triangulations of \mathbb{D} such that all triangles $\tau \in \mathcal{T}^{(n)}$ have diameter no greater than $1/n$, and for every n there is some $\tau_n \in \mathcal{T}^{(n)}$ such that f reverses the orientation of the vertices of τ_n . On a subsequence there is a limit point $\tau_n \rightarrow z_0 \in \mathbb{D}$. By the restriction on the similarity classes, there is a uniform upper bound c' to the ratio of any two sides of τ_n . In a suitable neighborhood U of z_0 the linear

approximation

$$|f(z) - f(z_0) - (J_f|_{z_0})(z - z_0)| \leq \frac{1}{3c} |z - z_0|,$$

is valid. For large n , $\tau_n \subseteq U$, and the inequality implies that that f sends the vertices of τ near to their images under the affine-linear mapping $f(z_0) + (J_f|_{z_0})(z - z_0)$, contradicting the property of reversing the orientation. This proves the affirmation. \square

5.3 Proof of main theorem

We divide the proof into several steps.

(1.) By standard approximation arguments we may replace $\mu(z)$ with $\mu(rz)$ for $r < 1$ arbitrarily close to 1, and thus we may suppose that μ is C^1 -smooth in a neighborhood of $\overline{\mathbb{D}}$. By Lemma 5.5, the solution $f = f_\mu$ of $(\partial f / \partial \bar{Z}) / (\partial f / \partial Z) = \mu$, which is indeed of class C^2 , sends sufficiently fine triangulations to triangulations. Statement (i) of the theorem will follow when we prove that the algorithm produces a sufficiently good approximation to f .

The pullback ν of μ given by (13) is C^1 in the closed left half-plane and is periodic of period $2\pi i$, while the solution $F = F_\nu$ of $(\partial F / \partial \bar{Z}) / (\partial F / \partial Z) = \nu$ is C^2 there, with the limiting conditions $F(-\infty) = -\infty$, $F(0) = 0$. Note that in general the extension of F by reflection in the imaginary axis is not C^1 on the axis.

The growth condition (26) implies that

$$r_{-M} < \frac{1}{N}, \tag{27}$$

so further

$$|z_{-M,k} - z_{-M,k-1}| < \frac{2\pi}{N} r_{-M} = O\left(\frac{1}{N^2}\right) \tag{28}$$

where $M = M_s$, $N = N_s$, $s \rightarrow \infty$.

(2.) We recall that the statement “ $AV = B$ ” in step 3 of the Algorithm translates roughly into the statement that “the PL-mapping $Z \mapsto W$ is $\{\nu_{jk}\}$ -conformal”. However, the algorithm only produces the Least-Squares approximation for (A, B) , which we will call V' ; i.e., the L_2 -norm $\|R'\|_2$ of the residual vector

$$R' = AV' - B \tag{29}$$

is the smallest possible.

We now restrict our attention to the mesh \mathcal{T}_{MN} . Consider the vector V defined by

$$\underline{V} = W = F(\mathcal{T}_{MN}). \tag{30}$$

which contains the images of the vertices under the true ν -conformal mapping F . By Lemma 5.5, W is a triangulation when the values M, N are large enough.

Fix such M, N , and let $\nu_{MN} = \{(\nu_{MN})_{jk}^\pm\}$ denote the collection of average values of the function ν on the triangles of \mathcal{T}_{MN} . Recall that the associated linear system $(A, B) = (A_{MN}, B_{MN})$ used in the algorithm is defined in terms of the values of ν_{MN} .

Let F_{MN}^* denote the PL-mapping on the support of \mathcal{T}_{MN} defined by the condition $\mathcal{T}_{MN} \rightarrow \underline{V}$. Thus by construction F_{MN}^* coincides with F on the vertices of \mathcal{T}_{MN} (both map to W), but the Beltrami derivative of F_{MN}^* is constant on each triangle. We will write ν_{MN}^* for this collection of constants.

Let (A^*, B^*) be the associated linear system to the discrete Beltrami coefficient ν_{MN}^* . We consider the following for fixed values of M, N :

$$AV' - B = R'. \quad (31)$$

$$A^*V - B^* = \varepsilon. \quad (32)$$

(3.) The vector $\varepsilon = \varepsilon_{MN}$ defined in (32) is described as follows. The entries of ε corresponding to the the triangle equations are 0 because F_{MN}^* is ν_{MN}^* -conformal and takes \mathcal{T}_{MN} to \underline{V} . Therefore the only nonzero values in ε are in the positions corresponding to the boundary equations. By (22) the values in A^*V are $F(Z_{-M,k}) - F(Z_{-M,k-1})$ while the values in B^* are $E_k - E_{k-1}$, so in the corresponding positions ε contains the value

$$(F(Z_{-M,k}) - E_k) - (F(Z_{-M,k-1}) - E_{k-1}).$$

To estimate this we recall f is of class C^2 and use the approximation

$$f(z) = (J_f|_0)(z) + O(|z|^2)$$

at the origin, where the Jacobian is given by $J_f|_0 = H_{a,0} \circ L_{\mu(0)}$ for some complex $a \neq 0$. From (28) we see that

$$\frac{f(z_{-M,k})e_{k-1}}{f(z_{-M,k-1})e_k} = \frac{e_k e_{k-1} + O(r_{-M}^3)}{e_k e_{k-1} + O(r_{-M}^3)} = 1 + O(r_{-M})$$

Taking logarithms we conclude that the nonzero entries of ε shrink at least as fast as $O(r_{-M})$. There are at most $2N$ nonzero entries, so (27) gives

$$\|\varepsilon_{MN}\|_2 = O\left(\left(\left(2N\right)\frac{1}{N^2}\right)^{(1/2)}\right) \rightarrow 0. \quad (33)$$

(4.) In practice, one applies the algorithm by using average values

$$\nu_{MN}(T) = \frac{\nu(Z_1) + \nu(Z_2) + \nu(Z_3)}{3}. \quad (34)$$

for $T = (Z_1, Z_2, Z_3) \in \mathcal{T}_{MN}$. It is a simple exercise to verify that this differs from the value $(\int_T \nu dx dy) / \text{area}(T)$ by an amount which tends to zero as $O(\delta^2)$, where

$\delta = \text{diam } T$. Since ν is differentiable, $\nu(Z_i) = \nu(Z_0) + (J_\nu|_{Z_0})(Z_i - Z_0) + O(\delta^2)$, $i = 1, 2, 3$, where we take $Z_0 = (Z_1 + Z_2 + Z_3)/3$. It is immediate from (34) that

$$\nu_{MN}(T) = \nu(Z_0) + O(\delta^2)$$

as the triangulation is refined and Z_0 always refers to the center of the triangle T .

On the other hand, consider

$$\begin{aligned} W_i &= F(Z_i) = F^*(Z_i) = W_0 + (J_f|_{Z_0})(Z_i - Z_0) + O(\delta^2) \\ &= W_0 + H_{a,b} \circ L_{\nu(Z_0)}(Z_i - Z_0) + O(\delta^2) \end{aligned} \quad (35)$$

(where the constants a, b depend on Z_0) and recall that $\nu_{MN}^*(T)$ is given by Corollary 2.3, i.e.,

$$\begin{aligned} \nu_{MN}^*(T) &= -\frac{(Z_2 - Z_1)(W_3 - W_1) - (Z_3 - Z_1)(W_2 - W_1)}{(\overline{Z_2} - \overline{Z_1})(W_3 - W_1) - (\overline{Z_3} - \overline{Z_1})(W_2 - W_1)} \\ &= \nu(Z_0) + O(\delta) \end{aligned}$$

as is seen by applying (2)–(3) in (35) and cancelling. We conclude that

$$|\nu_{MN}^* - \nu_{MN}| = O(\delta) = O\left(\frac{1}{N}\right). \quad (36)$$

(5.) The next step is to verify that

$$\|V\|_\infty = O(\log N). \quad (37)$$

The support $|\mathcal{T}_{MN}|$ of the Z -triangulation is a rectangle of width $R_M \approx \log N$ and height 2π . By (32), (33) we see that $\|A^*V - B^*\|_\infty$ can be made arbitrarily small by refining the mesh. This says that the triangles of \underline{V} are close to being ν_{MN}^* -conformal, so in particular the PL-mapping $F_{MN}^*: \mathcal{T}_{MN} \rightarrow \underline{V}$ is now known to be a local homeomorphism. We may think of the image as a Riemann surface extended over a region of the W -plane (Figure 4). This image is a possibly non-schlicht topological quadrilateral whose “vertical” sides are the lifting of the small ellipse together with its reflection in the imaginary axis. The “horizontal” sides are two curves shifted from one another by approximately $2\pi i$. If (37) were false, this quadrilateral would contain points W_s such that $\rho_s := |W_s|/\log N_s \rightarrow \infty$. This would imply that all curves joining the two vertical sides (see dotted curve in Figure 4) have Euclidean length at least $\rho_s \log N_s$. It follows from [18, Lemma 4.1], that the conformal module of this quadrilateral must also grow at least as fast as $\rho_s \log N_s$. Since $|\mathcal{T}_{MN}|$ has conformal module $O(\log N_s)$, the quasiconformal mappings F_{MN}^* must have arbitrarily large maximal dilatation; i.e., their Beltrami derivatives must have absolute value near to 1 at some point. This contradicts the fact that the Beltrami derivative is ν_{MN}^* , which is bounded away from 1 since it is close to ν . Therefore (37) holds as claimed.

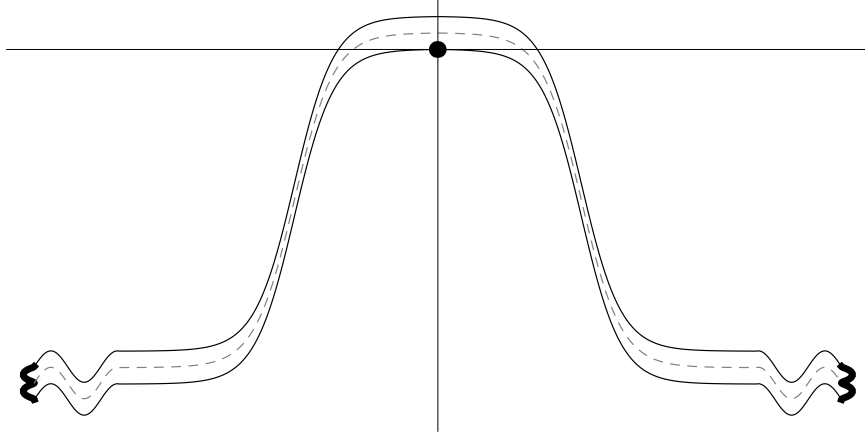


Figure 4: W -image containing points far from the origin. The lifted ellipse and its reflection are drawn as thicker curves for emphasis.

(6.) Now write

$$|A^* - A| = \sup |(A^*)_{jk} - (A)_{jk}|, \quad |B^* - B| = \sup |(B^*)_k - (B)_k|.$$

We observe that entries of (A, B) and (A^*, B^*) in a given position come from identical explicit formulas, with data ν_{MN}^* and ν_{MN} respectively. By Corollary 2.2, entries in A, A^* resulting from triangle equations are of the form $L_\nu(Z_i - Z_j)$, $L_{\nu^*}(Z_i - Z_j)$, respectively, where a given triangle is referred to by (Z_1, Z_2, Z_3) as in (34), and ν, ν^* refer to the constant values assigned to that particular triangle. The difference is

$$\begin{aligned} L_\nu(Z_i - Z_j) - L_{\nu^*}(Z_i - Z_j) &= \frac{2(\nu^* - \nu)\text{Im}(Z_i - Z_j)}{(1 + \nu)(1 + \nu^*)} \\ &= O\left(\frac{1}{N^2}\right) \end{aligned}$$

by (36), since $|\nu|$ is bounded away from 1. The entries of A, A^* resulting from boundary equations do not depend on ν, ν^* . We arrive at

$$|A^* - A| = O(1/N^2), \quad |B^* - B| = O(1/N), \quad (38)$$

the latter estimate resulting from a simple calculation based on (22).

Next we observe that by (32).

$$\begin{aligned} \|AV - B\|_2 &\leq \|AV - A^*V\|_2 + \|A^*V - B^*\|_2 + \|B^* - B\|_2 \\ &= \|(A - A^*)V\|_2 + \|\varepsilon\|_2 + \|B^* - B\|_2. \end{aligned}$$

By construction, each row of A or A^* contains at most three nonzero entries, as only three variables appear in equations (15), (17), etc. The entries of $(A - A^*)V$ are of the form $\sum_p (A_{pq} - A_{pq}^*)V_p$, where for each q , at most three of the

summands are nonzero. Thus $\|(A - A^*)V\|_\infty \leq 3|A - A^*| \|V\|_\infty = O(\log N/N^2)$ by (37) and (38). This vector has n_e elements, so we may estimate its L_2 -norm,

$$\begin{aligned} \|(A - A^*)V\|_2 &= O\left(\left(n_e\left(\frac{\log N}{N^2}\right)^2\right)^{1/2}\right) = O\left(\left(N^3\frac{1}{N^4}\right)^{1/2} \log N\right) \\ &= O(N^{-1/2} \log N) \rightarrow 0. \end{aligned}$$

A similar calculation shows that $\|B^* - B\|_2 \rightarrow 0$. By minimality of $\|AV' - B\|_2 = \|R'\|_2$ (recall (29)) and by (33), we have

$$\|R'\|_\infty < \|R'\|_2 \leq \|AV - B\|_2.$$

Therefore we have proved that $\|R'\|_\infty \rightarrow 0$. We will have no further need of the L_2 -norm in the discussion.

(7.) By (31) and (32),

$$\begin{aligned} \|A^*(V - V')\|_\infty &\leq \|A^*V - B^*\|_\infty + \|B^* - B\|_\infty + \|B - AV'\|_\infty \\ &\quad + \|AV' - A^*V'\|_\infty \\ &= \|\varepsilon\|_\infty + \|B^* - B\|_\infty + \|R'\|_\infty \\ &\quad + \|(A - A^*)V'\|_\infty. \end{aligned} \tag{39}$$

The fact $\|AV' - B\|_\infty \rightarrow 0$ tells us that the PL-mapping $\mathcal{T}_{MN} \rightarrow W' = \underline{V}'$ has bounded dilatation. As we showed in (37) for V , it follows also that $\|V'\|_\infty = O(\log N)$. Thus we may conclude that $\|(A - A^*)V'\|_\infty \rightarrow 0$ (again we need the fact that the rows of A^* have no more than three nonzero entries), so (39) implies that $\|A^*(V - V')\|_\infty \rightarrow 0$. By Lemma 5.3 (applied to A^* in place of A), we see that $\|V - V'\|_\infty$ (as determined by M_s, N_s) tends to zero as $s \rightarrow \infty$. This says that the points $W' = \underline{V}'$ produced by the algorithm differ by an arbitrarily small amount from the image vertices under the true ν -conformal mapping $W = F(Z)$.

(8.) Finally, we apply the exponential mapping via (6) and (7) to obtain the sequence of PL-mappings $f^{(s)}: z \mapsto w$ of subdomains which exhaust the unit disk \mathbb{D} , produced by the algorithm for the meshes determined by (M_s, N_s) . Let $\epsilon > 0$, and consider the annulus $\mathbb{D}_\epsilon = \{\epsilon < |z| < 1\}$. The image $f(\mathbb{D}_\epsilon)$ is approximately the part of \mathbb{D} outside of a small ellipse. By construction, the correspondence $F: Z \mapsto W$ extends by $2\pi i$ -periodicity to a mapping of the left half-plane $\{\operatorname{Re} Z \leq 0\}$ to $\{\operatorname{Re} W \leq 0\}$, as do all the approximants $F^{(s)}$. The extended quasiconformal mapping F is uniformly continuous on the band $\{-1/\epsilon \leq \operatorname{Re} Z \leq 0\}$, so the diameters of the W -triangles in the images of triangles contained in this band tend uniformly to zero as $s \rightarrow \infty$. Consider such a triangle (W_1, W_2, W_3) and its image (w_1, w_2, w_3) where $w_i = \exp W_i$. We compare the angle at W_1 , which is $\arg(W_3 - W_1)/(W_2 - W_1)$, with the angle

$$\arg \frac{w_3 - w_1}{w_2 - w_1} = \arg \left(\frac{e^{(W_1+W_3)/2}}{e^{(W_1+W_2)/2}} \cdot \frac{\sin(W_3 - W_1)}{\sin(W_2 - W_1)} \right)$$

at w_1 . The first factor on the right-hand side is $e^{(W_3 - W_2)/2} \rightarrow 1$ since $|W_3 - W_2| \rightarrow 0$. The second factor tends to $(W_3 - W_1)/(W_2 - W_1)$, again uniformly in the band. As a consequence, the exponential mapping sends W -triangles to approximately similar w -triangles (thus in particular respecting the orientation), and the procedure provides a triangulation of $f^{(s)}(\mathbb{D}_\epsilon)$ for which the induced PL-mapping $f^{(s)}|_{\mathbb{D}_\epsilon}$ is approximately μ -conformal. The limit as $s \rightarrow \infty$ is μ -conformal, fixes $z = 1$, and hence coincides with the mapping of doubly connected domains $f|_{\mathbb{D}_\epsilon}: \mathbb{D}_\epsilon \rightarrow f(\mathbb{D}_\epsilon)$. Since ϵ is arbitrary, we conclude that $f^{(s)} \rightarrow f$. This completes the proof. \square

6 Numerical Results

All of the calculations have been done with machine precision in *Mathematica* on a standard laptop computer of approximately 1GH. We have not found any examples where more precision will make a difference. The *Mathematica* routine `LeastSquares` handles sparse matrices [4, 26], a data structure which registers only the nonzero entries appearing in a matrix or vector.

In the first several examples we compare the results produced by our algorithm with an exact formula for the quasiconformal mapping under consideration.

Example 1. A simple test case is for constant $\mu(z) = c$. There is an explicit formula [25] for the conformal mapping to \mathbb{D} from an ellipse with semimajor and semiminor axes of lengths a, b ($a^2 - b^2 = 1$) and foci at ± 1 ,

$$w = \sqrt{k} \operatorname{sn} \left(\frac{2K}{\pi} \sin^{-1} u; k^2 \right) \quad (40)$$

where the Jacobi elliptic function modulus k is related to the complete elliptic integral K and the Jacobi theta functions by the formulas

$$q = (a + b)^{-4} = e^{-\pi K(1-m)/K(m)},$$

$$k = \sqrt{m} = \left(\frac{\theta_2}{\theta_3} \right)^2,$$

with notation from [27]. Note that the image of the circle $|z| = 1$ under the mapping L_μ is an ellipse with semiaxes $1, (1 - |\mu|)/(1 + |\mu|)$ slanted in the directions $(1/2)\arg \mu, (1/2)(\arg \mu + \pi)$ respectively, modulo π . This ellipse is sent by the conformal linear mapping $H_{1/(2\sqrt{\mu}), 0}$ to the ellipse with semiaxes a, b . Then via (40) this is transformed conformally to the unit disk.

It is well known that a conformal mapping from an ellipse to a disk tends to “crowd” boundary points near the images of the endpoints of the major axis. The crowding, or maximum ratio of separation of N points sent to the N th roots of unity, increases exponentially as a function of the aspect ratio a/b [10, section 2.6]. In contrast, the affine mapping L_μ which we combined with this

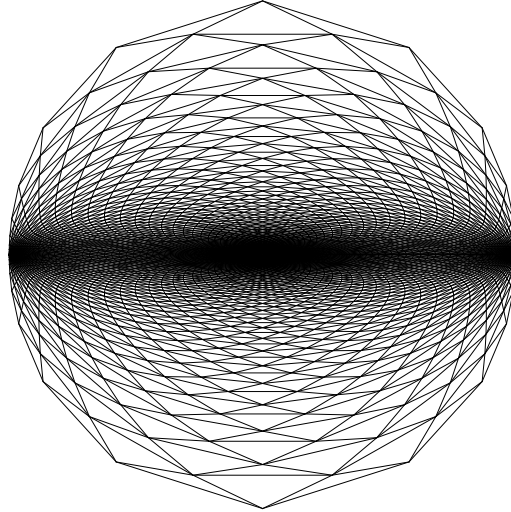


Figure 5: Image for constant Beltrami derivative $\mu = 0.5$ and $(M, N) = (52, 64)$. Observe the “crowding phenomenon” at the boundary.

conformal mapping produces little crowding. The combined effect is a great deal of crowding near $w = 1$, as can be perceived in Figure 5.

The algorithm of Theorem 5.1 was applied for the constant Beltrami derivatives $\mu = 0.1, 0.3, 0.5, 0.7$, and meshes defined by $N = 16, 32, 48, 64, 72, 84$, with M equal to the least multiple of 4 no less than $N \log N / (\pi\sqrt{3})$, in view of (26). In the last case there are 24359 equations in 14196 variables. It took about 1.5 seconds to calculate the part of the matrix in the left half-plane, and about 10 seconds to solve the full set of equations. Table 1 presents the maximum error over all w_{kj} when these points are compared to the images of z_{kj} under the exact quasiconformal mapping described in the preceding paragraph. As is to be expected, the error increases when the Beltrami derivative increases, but decreases when the mesh is refined. It was found that for $\mu = 0.7$ and a rather coarse mesh such as $(M, N) = (36, 48)$, the image of \mathcal{T}_{MN} is not a triangulation, inasmuch as a few of the w -triangles near ± 1 are improperly oriented. In spite of this fact, the values obtained for the conformal mapping are not very far off.

(M, N)	(12,16)	(24,32)	(36,48)	(52,64)	(60,72)	(72,84)
$\mu = 0.1$	0.012	0.0031	0.0014	0.0008	0.0006	0.0004
$\mu = 0.3$	0.0274	0.007	0.0031	0.0018	0.0014	0.001
$\mu = 0.5$	0.0615	0.0205	0.0109	0.0065	0.0051	0.0038
$\mu = 0.7$	0.2439	0.1201	0.0856	0.0627	0.053	0.0412

Table 1: The maximum of the absolute errors between the solutions and the real values of some constant Beltrami derivative and $M \approx N \log N / (\pi\sqrt{3})$.

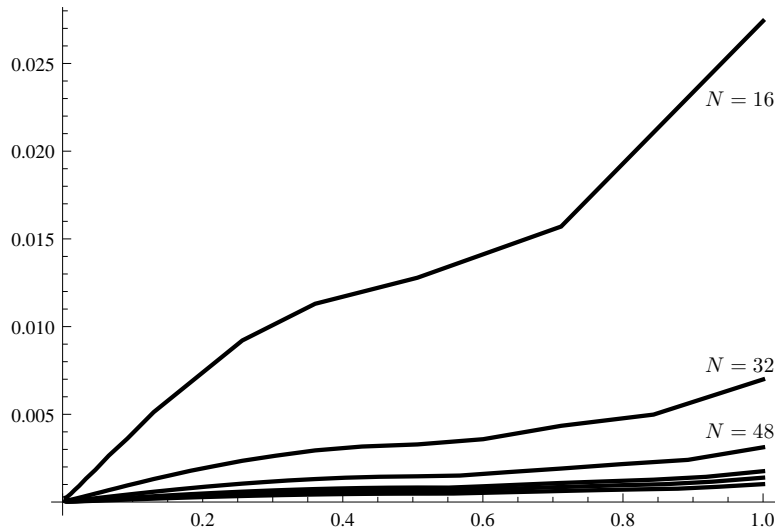


Figure 6: Numerical errors of algorithm for different values of (M, N) with $\mu = 0.3$. The horizontal axis indicates the distance $r_j = |z_{jk}|$ of the z -points from the origin; the vertical axis gives the maximum discrepancy (over k) of the calculated value of w_{jk} from the true value.

We give a further analysis of the variation of the error as a function of the radius, for the particular value $\mu = 0.3$. Figure 6 shows the maximum error over k in the calculated value of w_{jk} for each fixed j . It is seen that the error remains approximately constant for $r < 0.7$ and then increases rather sharply for $0.7 < r < 1$. Thus the maximum values in Table 1 are much higher than the average errors. As noted above, the maximum error, which occurs on the boundary, decreases as a function of N .

Example 2. *Radial quasiconformal mapping.* Let $\varphi: [0, 1] \rightarrow [0, 1]$ be an increasing diffeomorphism of the unit interval. Then the radially symmetric function

$$f(z) = \varphi(|z|)e^{i \arg z} = \varphi(|z|)\frac{z}{|z|} \quad (41)$$

has Beltrami derivative equal to

$$\mu(z) = \frac{|z|\varphi'(z)/\varphi(z) - 1}{|z|\varphi'(z)/\varphi(z) + 1} \frac{z}{\bar{z}} \quad (42)$$

when $z \neq 0$. As an illustration we will take

$$\varphi(r) = (1 - \cos 3r)/(1 - \cos 3)$$

as in Figure 7. The resulting Beltrami derivative satisfies $\|\mu\|_\infty = 0.65$ approximately.

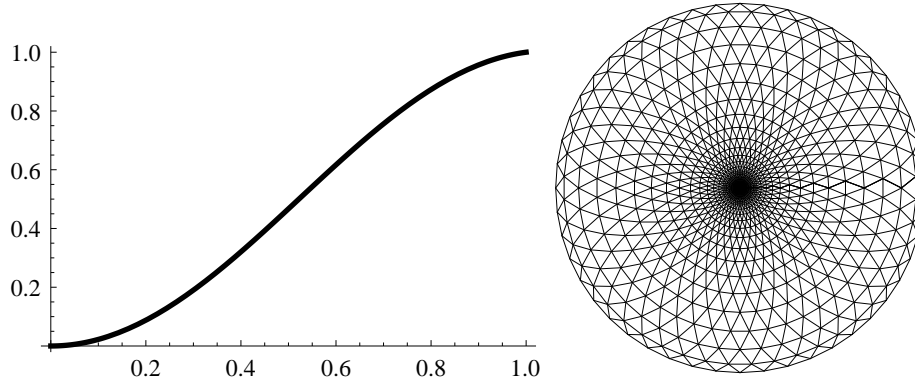


Figure 7: Radial function φ of example 2 (left), together with the induced rotationally symmetric image domain.

The domain points z_{jk} on the real axis were selected, and the values of w_{jk} produced by the algorithm were compared with the true values $\varphi(|z_{jk}|)$. The results are given in Table 2. It was also observed that as in the previous example, the errors increase as the radius increases.

(M,N)	(12, 16)	(24, 32)	(36, 48)	(52, 64)	(60, 72)	(72, 84)
Error	0.0398	0.0135	0.0058	0.0034	0.0027	0.0020

Table 2: Maximum absolute error for radially symmetric with μ mapping defined by (42).

Example 3. *Sectorial quasiconformal mapping.* In a similar spirit, we let $\psi: [0, 2\pi] \rightarrow [0, 2\pi]$ be an increasing diffeomorphism. Write $\tilde{\psi}(e^{i\theta}) = e^{i\psi(\theta)}$. Then the sectorially symmetric function

$$f(z) = |z| \tilde{\psi} \left(\frac{z}{|z|} \right) \quad (43)$$

has Beltrami derivative equal to

$$\mu(z) = \frac{1 - \psi'(\theta)}{1 + \psi'(\theta)} \frac{z}{\bar{z}} \quad (44)$$

when $z \neq 0$. As an example we will take

$$\psi(\theta) = \begin{cases} \frac{\theta}{2}, & 0 \leq \theta \leq \pi, \\ \frac{\pi}{2} + \frac{3(\theta - \pi)}{2}, & \pi \leq \theta \leq 2\pi. \end{cases}$$

as in Figure 8. In this example μ does not satisfy the hypotheses of Theorem 5.1 because it is not continuous. The arguments of the final boundary values on the unit circle were compared with the true values $\psi(\theta)$; see Table 3.

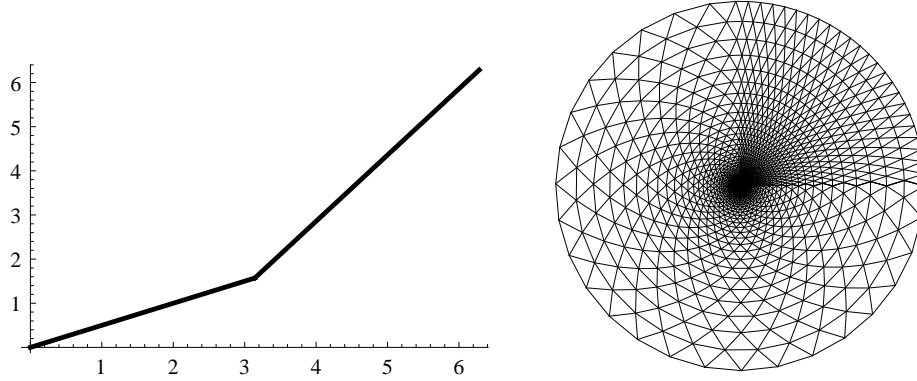


Figure 8: Angular function ψ of example 3 (left), together with image domain under sectorial mapping (43).

(M,N)	(12, 16)	(24, 32)	(36, 48)	(52, 64)	(60, 72)	(72, 84)
Error	0.0712	0.0362	0.0251	0.0193	0.0173	0.0150

Table 3: Maximum absolute error $|\psi(\theta) - f(e^{i\theta})|$ for sectorial mapping with μ defined by (44).

Example 4. Exterior mappings. In Daripa [7], quasiconformal mappings from \mathbb{D} to the exterior of an ellipse (the origin being sent to ∞) are calculated with the following two sample Beltrami derivatives,

$$\mu_1(z) = |z|^2 e^{0.65(iz^5 - 2.0)},$$

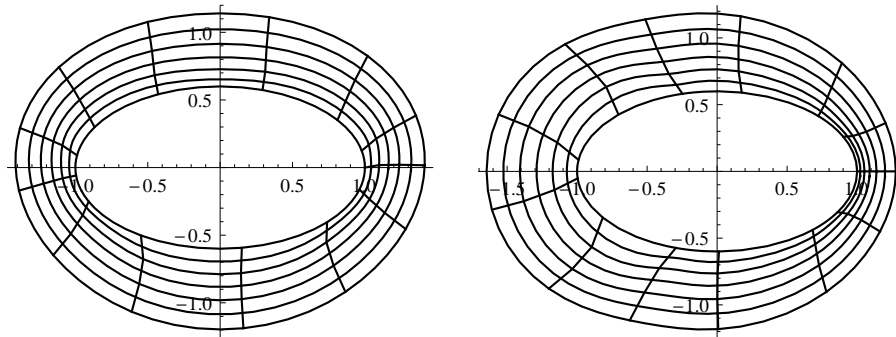


Figure 9: Self-mappings of unit disk with Beltrami derivatives μ_1 (left), μ_2 (right) followed by conformal mapping to exterior of ellipse as in [7].

$$\mu_2(z) = \frac{1}{2}|z|^2 \sin(5\operatorname{Re} z).$$

These exterior mapping results can be related to those of our algorithm by use of the rational function

$$h(z) = \frac{(1 + \alpha) - (1 - \alpha)z^2}{2\alpha z}$$

which transforms \mathbb{D} conformally to the exterior of an ellipse with aspect ratio α . Composition of h following the quasiconformal self-mapping of D provides a mapping to the exterior of the ellipse with the same Beltrami derivative.

In the examples in [7], $\alpha = 0.6$ is specified (however, the inner ellipses in [7] appear to have aspect ratios of approximately 0.47; axes are not drawn.) We have made adjustment for the fact that Daripa uses M radii equally spaced in $[0, 1]$, in contrast to the exponential spacing we have been using. Our results are depicted in Figure 9 with $(M, N) = (64, 64)$. These images appear fairly similar those shown in [7].

Computation times are reported in [7] for $N = 64$ as approximately 8.5 seconds of CPU on a MIPS computer described as “approximately 15 times slower than the CRAY-YMP at Texas A & M University” of that time. Our laptop CPU times, using *Mathematica*, were approximately 15 seconds for the first example and 45 seconds for the other.

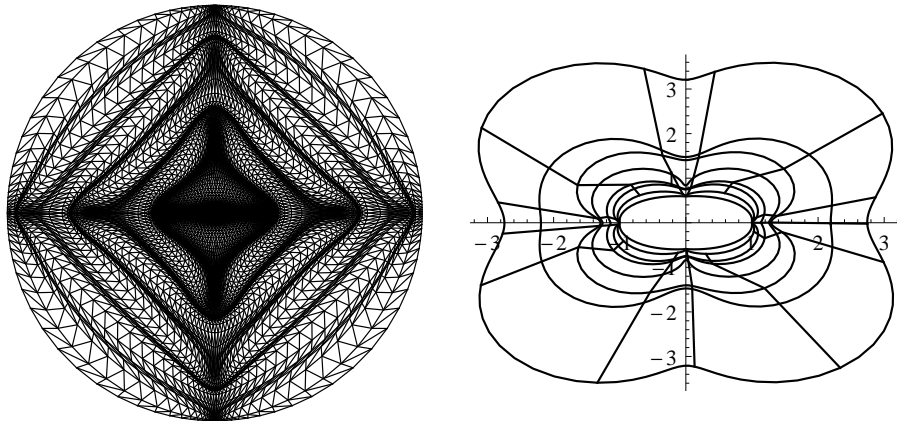


Figure 10: Quasiconformal mappings to disk (left) and exterior of ellipse (right) determined by (45).

It is apparent from the examples in [7] that Beltrami derivatives with a great deal of oscillation were used in order to create an interesting problem. Figure 10 shows our results for the mapping of the disk to the exterior of the same ellipse, with Beltrami derivative

$$\mu(z) = 0.9 \sin |20z| \tag{45}$$

and $(M, N) = (128, 128)$.

(5) *Quasiconformal deformation of Fuchsian groups.* In this example μ is associated to a quadratic differential for a Fuchsian group (see [13, 17] for definitions). The two linear-fractional transformations

$$z \mapsto \frac{z + \sqrt{2}/2}{(\sqrt{2}/2)z + 1}, \quad z \mapsto \frac{z + i\sqrt{2}/2}{-i(\sqrt{2}/2)z + 1}$$

generate a free group Γ of self-mappings acting freely on \mathbb{D} . This group has a standard fundamental domain with four-fold symmetry about the origin as shown in Figure 11, and the quotient Riemann surface \mathbb{D}/Γ is homeomorphic to a torus with a single puncture. We create a holomorphic function in \mathbb{D} via the Poincaré series

$$\Theta(z) = \sum_{\gamma \in G} (\gamma'(z))^2. \quad (46)$$

which is known to converge and to satisfy the invariance relation

$$\Theta(\gamma(z))\gamma'(z)^2 = \Theta(z) \quad (47)$$

for every γ in Γ . Then for $0 \leq |c| < 1$ the function

$$\mu(z) = c \frac{\overline{\Theta(z)}}{\Theta(z)} \quad (48)$$

is a Beltrami differential for the group Γ ; that is, $\mu(\gamma(z))\overline{\gamma'(z)}/\gamma'(z) = \mu(z)$ for every γ in Γ . This implies that the normalized μ -conformal self-mapping $f_c: \mathbb{D} \rightarrow \mathbb{D}$ satisfies $f_c(\gamma(z)) = \gamma_c(f_c(z))$ where $\gamma \mapsto \gamma_c$ is an isomorphism from Γ to another Fuchsian group Γ_c also acting on \mathbb{D} . A large part of Teichmüller

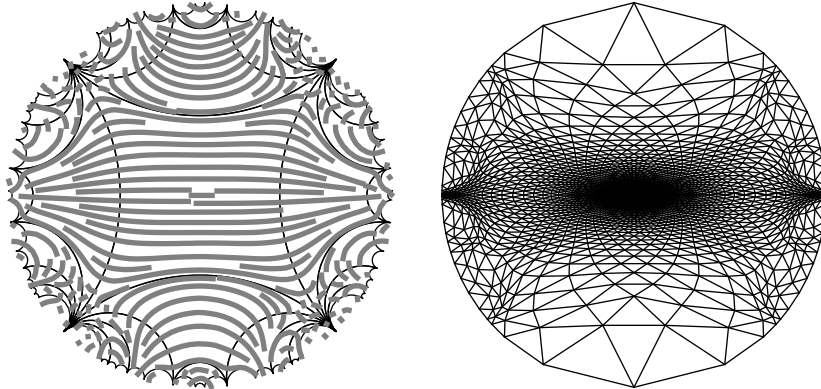


Figure 11: (left) Horizontal trajectories of quadratic differential Φ (46); (right) image triangulation arising from induced Teichmüller differential (48), which effectively produces a stretching along these trajectories.

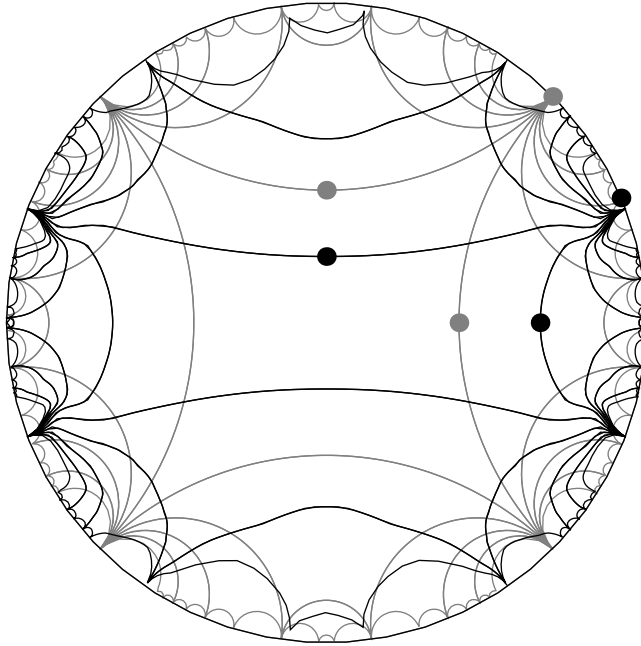


Figure 12: Self-mapping of unit disk, with Beltrami derivative defined via a Poincaré series. Computations were made with $(M, N) = (64, 64)$. The standard fundamental domain (lighter contour) is symmetric under rotation by $\pi/2$; its image under the quasiconformal mapping (black contour) is superimposed.

theory is devoted to understanding the nature of deformed groups such as Γ_c and their dependence on μ .

Figure 11 shows the trajectory structure of the quadratic differential Φ , that is, the solutions of $\Phi(z)dz^2 > 0$, together with a w -triangulation obtained from the μ -conformal mapping for $c = 0.5$. Figure 11 shows the w -triangulation for $(M, N) = (64, 64)$. Figure 12 is a superposition of the z - and w -domains, with part of the tessellation of \mathbb{D} by group translates of the fundamental domain of Γ and also the tessellation by their images, which are fundamental domains for Γ_μ . The images were calculated by taking each point defining each curve of the original tessellation, identifying the particular z -triangle in which it lies, and then applying the PL-mapping to the corresponding w -triangle of Figure 11. Some inaccuracies, particularly near the boundary, are clearly visible inasmuch as the image curves must be hyperbolic geodesics. One probable source of error is in the calculation of $\Theta(z)$. To evaluate (46) we truncated the series to words of up to length 6 in the generators of Γ and/or inverses, and used (47) to apply (46) directly only for z inside the fundamental domain containing the origin; then (48) was applied for points outside the fundamental domain.

An independent verification of this mapping is made using the results of

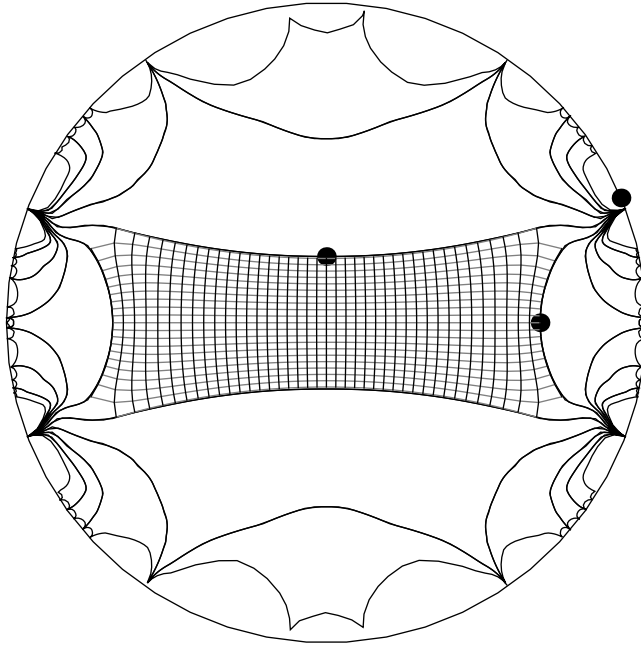


Figure 13: Comparison of the image of the basic fundamental domain via quasiconformal mapping and conformal mapping techniques. The trajectories inside the fundamental domain were calculated as the images under the conformal mapping of vertical and horizontal segments in the period rectangle of the Weierstrass \wp -function.

[5] on conformal mapping of symmetric quadrilaterals with circular sides. In the present context, where the vertex angles of the fundamental domains are all equal to zero, such quadrilaterals depend (up to conformal equivalence) on two real parameters, which may be prescribed in several ways, some relating to the geometry of the circular quadrilateral (such as the midpoints p_1, p_2 of the right and upper edges as marked in Figure 12), others relating to parameters in the conformal mapping. In particular, there is a conformal mapping h from a Euclidean rectangle with vertices at $\pm\omega_1 \pm \omega_2$ ($\omega_1 > 0, \omega_2/i > 0$) to the fundamental domain quadrilateral, whose Schwarzian derivative \mathcal{S}_h [1] is equal to the following elliptic function:

$$\mathcal{S}_h(\zeta) = \frac{1}{2}\wp(\zeta + \omega_1 + \omega_2) - 2\sigma, \quad (49)$$

where the essential parameter is the purely imaginary ratio $\tau = \omega_2/\omega_1$, which determines the second parameter $\sigma = \sigma(\tau) \in \mathbb{R}$ due to the fact that the circular edges must be orthogonal to the circle passing through the four image vertices $h(\pm\omega_1 \pm \omega_2)$. Here ω_1, ω_2 are basic half-periods of the Weierstrass \wp -function, normalized in a specific way which we will not describe here. Methods are given in [5] for calculating the relationships among these parameters. We have applied

them to the observed values for $p_1 = f_c(\sqrt{2}-1)$ and $p_2 = f_c(i(\sqrt{2}-1))$ obtained from our algorithm for the Beltrami equation, together with the fact that $\tau = (1-c)/(1+c)$, to obtain the value of σ numerically. Then the Schwarzian differential equation (49) was solved, first along the real and imaginary axes, and from there along vertical and horizontal lines throughout the rectangle with vertices $\pm\omega_1 \pm \omega_2$. Since this was done with a normalization of $h'(0) = 1$, a further scaling was necessary to adjust the size to match the value of p_1 . It is seen (Figure 13) that the midpoint p_2 and the curvatures of the edges agree quite well. In general if one is interested in deforming Fuchsian or Kleinian groups by this method, a reasonable strategy would be to replicate the information obtained in such a fundamental domain via the group action of Γ_c .

c	τ	$N = 16$	$N = 32$	$N = 48$	$N = 64$
0.1	0.818	0.022	0.006	0.003	0.002
0.3	0.538	0.089	0.027	0.011	0.008
0.5	0.333	0.283	0.110	0.052	0.031

Table 4: Relative error of midpoint p_2 of the upper edge of the deformed fundamental domain compared to result of conformal mapping from rectangle. Calculations made with $M = N$.

7 Discussion and Conclusions

It is stated in Daripa [7] that prior to that article there were no constructive methods published for solving the Beltrami equation in the disk numerically. Convergence proofs appeared later in [11] together with a modified scheme. There are other methods which also include convergence proofs (we have mentioned [14, 28]) without giving a detailed analysis of the rate of convergence. Therefore we discuss here some aspects of [7, 11] in relation to our algorithm. As we mentioned in the Introduction, that approach is based on evaluation of singular integrals. The original problem is presented in the context of finding a μ -conformal mapping to a prescribed star-shaped domain, and is in some ways reminiscent of the classical method of Theodorsen [15] for conformal mappings.

Daripa's main algorithm requires evaluation of the $\partial/\partial\bar{z}$ derivatives which appear in the singular integrals. A variant is also proposed which does not require these derivatives; however this is not applied in the numerical examples provided. The operation count of one iteration of Daripa's method is $O(MN \log N)$. This should be multiplied by the average number of iterations required, which depends on how refined the mesh is and how much accuracy is desired. In the examples which we have taken from [7], $\|\mu\|_\infty$ is approximately 0.5, but it should be noted that $|\mu(z)|$ is in fact bounded by 0.12 for $|z| < 0.5$, and by 0.05 for $|z| < 0.3$. In fact, an important limitation stated in [7] is that the Beltrami derivative μ must be Hölder continuous. Further, it is recommended that μ vanish at least as fast as $|z|^3$ at the origin for the method to work prop-

erly. In [11] it is similarly recognized that computation time increases as $\|\mu\|_\infty$ increases. Our algorithm, in contrast, is not subject to any such requirement on μ . Our computation times are considerably longer than those reported in [11] but this may be due in large part to use of a symbolic interpreter rather than a compiled program.

We also mention the method presented in [21] for determining a Teichmüller mapping to an arbitrary domain. It begins by choosing an “optimal” Beltrami derivative and then solving the corresponding boundary Beltrami equation. A system of linear equations is determined to discretize this equation, which must be solved together with a collection of nonlinear boundary constraints. This is solved by an iterative method (conjugate gradient).

Our algorithm involves no evaluation of singular integrals and no iteration of solutions. As described in Section 5, we use a purely linear system (A, B) . For a mesh of dimensions M, N , the matrices A, B are of orders $n_e \times n_v, n_e \times 1$ respectively, where $n_e = 4MN + 2(N - 1) + 1$ and $n_v = (2M + 1)N$. Although the total number of elements contained in A is $O(M^2N^2)$, by construction A is a sparse matrix: as we noted during the proof of Theorem 5.1, the number of nonzero elements of any row of A is no greater than 3; further, the number of nonzero elements of any column of A is no greater than 7 (note that each variable W_{jk} in (15), (17) corresponds to a vertex of at most six triangles, cf. Figure 1; the only vertex appearing in seven equations is $W_{0,0}$, cf. (23)). Hence the number of nonzero elements in A is no greater than $O(MN)$.

Since the linear system $AV = B$ is highly overdetermined and in general there is no exact solution, we use the least squares approximation. There are many numerical methods available for the least squares problem; a comprehensive reference is [4]. For simplicity we discuss the method of “normal equations,” that is, the solution of $A^H AV = A^H B$, where A^H is the conjugate transpose of A . It is easily seen that by construction the columns of A are linearly independent, so that $A^H A$ is positive definite, and each row or column of $A^H A$ contains at most 7 nonzero entries. These entries are not consecutive, but the index correspondence in (24) may be taken so that the row bandwidth of $A^H A$ is $2M$. When one applies Gaussian reduction to (A, B) , the n th of the n_v rows will only need to reduce at most $2M$ of the succeeding rows, and will require no more than $2M$ floating-point multiplications for each one. Thus the total operation count is of the order of $O(n_v(2M)^2) = O(M^3N)$. Once $A^H A$ has been thus reduced to echelon form, the computational cost of back substitution is seen to be no more than $O(M^2N)$. These computations do not require a significant amount of storage other than the original data. In summary, when one doubles the mesh dimensions M, N , the memory requirement is at most multiplied by 4 (which is the same as the increase in the mesh itself) and the computation time by 16. Our numerical experiments indicate that the more sophisticated least-squares algorithms found in packaged software appear to reduce these exponents slightly.

It may be noted that our algorithm can be used for solving the Beltrami

equation on the entire z -plane (normalized by fixing 0, 1, and ∞) instead of the disk. One simply eliminates the step of extending the Beltrami coefficient from the disk to its exterior by reflection. We have not yet investigated this question numerically. Further, it seems probable that our algorithm will converge to the μ -conformal mapping even when μ is only piecewise smooth, and perhaps in even greater generality. Many numerical examples suggest this, some of which we have given above. The estimates in the proof of Theorem 5.1 concerning L_2 norms would not be greatly affected if only a small proportion of the terms in the sums failed to tend to zero as fast as required. We hope to look into these questions in future work.

We believe that this algorithm for solving the Beltrami equation is conceptually much simpler than other methods which have been presented, and is easy to implement.

The authors are grateful to T. Sugawa for many critical and useful comments in the preparation of this work. The first author is also grateful to D. Marshall for pointing out several fundamental errors in the approach proposed in [23].

References

- [1] L. Ahlfors, *Lectures on Quasiconformal Mappings*, second edition, University Lecture Series **38**, American Mathematical Society, Providence, RI (2006).
- [2] S. Angenent, S. Haker, A. Tannenbaum, and R. Kikinis, Laplace-Beltrami operator and brain surface flattening, *IEEE Trans. Medical Imaging* **18**:700–711 (1999).
- [3] K. Astala, J. L. Mueller, A. Perämäki, L. Päivärinta, and S. Siltanen. Direct electrical impedance tomography for nonsmooth conductivities, *Inverse Problems and Imaging* **5**:531–549 (2011).
- [4] Å. Björck, *Numerical Methods for Least Squares Problems*, SIAM. (1996) ISBN 978-0-89871-360-2.
- [5] P. Brown and R. M. Porter, Conformal mapping of circular quadrilaterals and Weierstrass elliptic functions, *Comput. Methods Funct. Theory* **11**:463–486 (2011).
- [6] P. Daripa and D. Mashat, An efficient and novel numerical method for quasiconformal domains, *Numer. Algorithms* **18**:159-175 (1998).
- [7] P. Daripa, A fast algorithm to solve the Beltrami equation with applications to quasiconformal mappings, *J. Comput. Phys.* **106**:355-365 (1993).
- [8] P. Daripa, On applications of a complex variable method in compressible flows, *J. Comput. Phys.* **88**:337–361 (1990).

- [9] P. Daripa, A fast algorithm to solve nonhomogeneous Cauchy-Riemann equations in the complex plane, *SIAM J. Sci. Statist. Comput.* **13**:1418–1432 (1992).
- [10] T. A. Driscoll and L. N. Trefethen *Schwarz-Christoffel mapping*, Cambridge Monographs on Applied and Computational Mathematics **8**, Cambridge University Press, Cambridge (2002).
- [11] D. Gaidashev, D. Khmelev, On numerical algorithms for the solution of a Beltrami equation, *SIAM J. Numer. Anal.* **46**:5 (2008) 2238–2253.
- [12] X. D. Gu, W. Zeng, F. Luo, and Sh-T. Yau, Numerical computation of surface conformal mappings, *Comput. Methods Funct. Theory* **11**:747–787(2011).
- [13] W. J. Harvey, ed. *Discrete Groups and Automorphic Functions. Proceedings of an Instructional Conference held in Cambridge, July 28–August 15, 1975*, Academic Press (1977).
- [14] Zh.-X. He, Solving Beltrami equations by circle packing, *Trans. A.M.S.* **322**:657–670 (1990).
- [15] P. Henrici, *Applied and Computational Complex Analysis*, vol. **3**, Wiley, New York (1986).
- [16] D. S. Kamenetskiĭ and S. V. Tsynkov, On the construction of images of simply connected domains realized by solutions of a system of Beltrami equations (Russian), *Akad. Nauk SSSR Inst. Prikl. Mat.* Preprint no. 155 (1990).
- [17] O. Lehto, *Univalent Functions and Teichmüller Spaces*, Springer-Verlag, New York (1995).
- [18] O. Lehto and K. I. Virtanen, *Quasiconformal Mappings in the Plane*, second edition, *Die Grundlehren der mathematischen Wissenschaften* **126** Springer-Verlag, New York-Heidelberg (1973).
- [19] B. Lévy, S. Petitjean, N. Ray and J. Maillot, Least Squares Conformal Maps for Automatic Texture Atlas Generation, *ACM Transactions on Graphics (TOG)*, Proceedings of ACM SIGGRAPH 2002 **21**:362–371 (2002).
- [20] L. M. Lui, K. C. Lam, T. W. Wong, and X. Gu, Texture Map and Video Compression Using Beltrami Representation, *SIAM J. Imaging Sci.* **6**:1880–1902 (2013).
- [21] L. M. Lui, K. C. Lam, S-T. Yau, and X. Gu, Teichmüller extremal mapping and its applications to landmark matching registration, [arXiv:1211.2569v1](https://arxiv.org/abs/1211.2569v1).

- [22] J. R. Munkres, *Elementary Differential Topology. Lectures given at Massachusetts Institute of Technology, Fall, 1961*. Revised edition. Annals of Mathematics Studies, No. 54 Princeton University Press, Princeton, N.J.
- [23] R. M. Porter, Numerical solution of the Beltrami equation, [arXiv:0802.1195](https://arxiv.org/abs/0802.1195) [math.CV]
- [24] Z. V. Samsoniya, Construction of certain quasiconformal mappings (Russian), *Trudy Vychisl. Tsentra Akad. Nauk Gruzin. SSR* **23**:76-89 (1983).
- [25] G. Szegő, Conformal mapping of the interior of an ellipse onto a circle, *American Mathematical Monthly* **57**:474–479 (1950).
- [26] M. Trott, *The Mathematica GuideBook for Numerics*, Springer Science+Business Media, Inc. (2006).
- [27] E. T. Whittaker and G. N. Watson, *A Course of Modern Analysis*, reprint of the fourth (1927) edition, Cambridge Mathematical Library, Cambridge University Press, Cambridge (1996).
- [28] G. B. Williams, A circle packing measurable Riemann theorem, *Proc. Amer. Math. Soc.* **134**:2139–2146 (2006).